Langmuir

Article

pubs.acs.org/Langmuir

Three-Dimensional Wax Patterning of Paper Fluidic Devices

Christophe Renault,[†] Jessica Koehne,[‡] Antonio J. Ricco,[§] and Richard M. Crooks*[,†]

[†]Department of Chemistry, Center for Nano- and Molecular Science and Technology, The University of Texas at Austin, 105 East 24th Street, Stop A5300, Austin, Texas 78712-1224, United States

[‡]Center for Nanotechnology and [§]Small Payloads and Instruments Group, NASA Ames Research Center, Moffett Field, California 94035-1000, United States

Supporting Information

ABSTRACT: In this paper we describe a method for three-dimensional wax patterning of microfluidic paper-based analytical devices (μPADs). The method is rooted in the fundamental details of wax transport in paper and provides a simple way to fabricate complex channel architectures such as hemichannels and fully enclosed channels. We show that three-dimensional μPADs can be fabricated with half as much paper by using hemichannels rather than ordinary open channels. We also provide evidence that fully enclosed channels are efficiently isolated from the exterior environment, decreasing contamination risks, simplifying the handling of the device, and slowing evaporation of solvents.

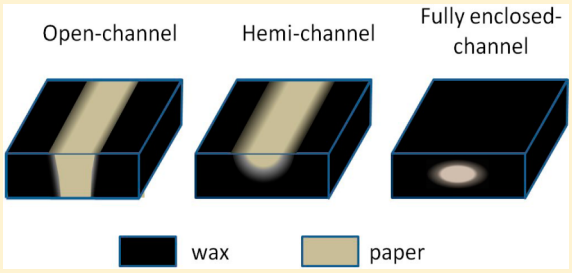

INTRODUCTION

Lateral-flow assay (LFA) devices, often made from a porous layer such as nitrocellulose supported on a nonporous polymer backing such as a film of polyester, are used commercially to conduct millions of low-cost diagnostic assays each day.[1] Fluid flows through LFA devices by passive capillary action and reagents are readily immobilized in lyophilized (or dried) form in the porous layer; the addition of a fluid sample or reagent redissolves them. Readout is often via visual assessment of a localized spot or line of color that forms due to binding of a target species and/or functionalized chromophore, although more sophisticated measurement systems that eliminate human judgment and provide quantitative outputs are now common.[1] In use for more than two decades, LFA devices generally rely upon the thickness of the supported porous layer and the width of the device, commonly referred to as a "test strip", to define and bound the flow of fluid. They do not include "microchannels" in the sense that this term is used in modern microfluidic systems, thereby limiting their flexibility and adaptability to more complex fluid manipulations or flow topologies that may be necessary for such tasks as preassay sample preparation or realization of multiplexed analysis of several target species.

Recently, the paper-based analytical device (μPAD) has been suggested as an alternative, complement, or improvement to LFA technology.[2,3] With the potential for similarly low costs of materials and manufacturing, μPADs replace nitrocellulose with more ordinary cellulose, or "paper", and eliminate the supporting polymer substrate. Most significantly, these devices include flow paths or microchannels prepared by patterning a hydrophobic material, such as photoresist or wax, onto/into hydrophilic cellulosic paper to define channels within the paper that are constrained by hydrophobic walls.[4] They also can be folded to create more complex fluidic topologies, a method referred to as microfluidic origami (see below).[19,20] Both differences from LFA enable more complex flow paths and microfluidic processes in μPADs. In operation, liquids move through the channels in μPADs via capillary action as in LFA devices; reagents for analysis can be immobilized on or within the paper channels by drying at a desired location. An analytical signal is produced when the sample containing the analyte contacts a particular reagent or is bound to an optically or electrochemically labeled recognition moiety. In many cases, the outcome of the analysis is signaled by a simple color change, and in this case, no power source is required to use the device.[4−6]

The first generation of μPADs, reported by Whitesides and co-workers,[5] used "open" channels that extend through the entire thickness of the paper substrate, as shown in column a of Scheme 1, to transport fluids. These devices were fabricated by impregnating chromatography paper with photoresist and then using photolithography to pattern the channel.[5] Since then, several other methods, including inkjet etching,[7] plasma etching,[8] cutting[9] (as for LFA devices), and wax patterning,[10−16] have been used to pattern hydrophilic channels in paper.

Wax patterning in particular offers several advantages over other fabrication methods. First, it is relatively rapid: in our laboratory, several hundred devices can be produced in less than 1 h, and at production scale this number would be orders of magnitude higher. In fact, with LFA technology a million or more devices per day can be made in a roll-to-roll processing

Received: March 30, 2014
Revised: May 20, 2014
Published: June 4, 2014

   dx.doi.org/10.1021/la501212b | Langmuir 2014, 30, 7030−7036

Scheme 1. Cross-Sectional Views of Wax-Patterned Substrates

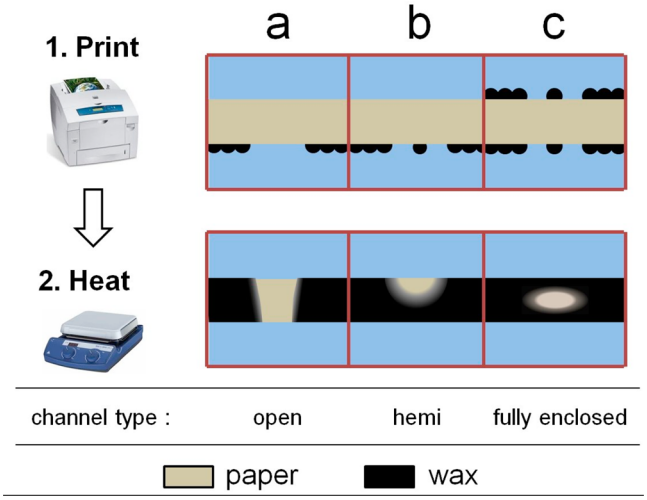

system. Second, the paper microchannel is not exposed to polymers or solvents during patterning, and therefore, the likelihood of contamination is reduced, while the process is potentially much less expensive because throughput can be far higher.[17] Third, wax patterning is remarkably easy to carry out. As shown in the top row of Scheme 1, wax is first printed onto the surface of the paper using a commercially available wax printer. Then the paper is heated to a relatively low temperature ($T \approx 110-130$ °C) to melt the wax and form the hydrophobic channel walls within the paper (Scheme 1, bottom row).

Although open channels, like that depicted in column a of Scheme 1, are the most commonly encountered design features in μPADs, other architectures exist. For example, Olkkonen et al. fabricated half-closed channels, which we call hemichannels (Scheme 1, bottom row of column b), by flexographically printing a thin layer of polystyrene on one side of the paper device.[18] Schilling et al. described a hybrid method that combines wax patterning and toner printing for fabricating fully enclosed channels similar to the one represented in Scheme 1, bottom row of column c.[19] In this case, an open channel was wax patterned and subsequently sealed on both sides by printing several layers of toner with a laser printer. Using an inkjet printer fed with UV-curable ink, Maejima et al. were also able to fabricate hemichannels and fully enclosed channels.[20]

The first 3D μPADs were also reported by Whitesides and co-workers,[21] who stacked individual, photolithographically patterned 2D μPADs together using double-sided tape. The channels were then hermetically sealed using tape. Connections between layers were established by laser drilling holes in the tape and filling the resulting vias with cellulose powder. We reported an alternative, simplified method for preparing 3D μPADs that is based on the principles of origami.[22,23] We call these devices origami paper-based analytical devices, or *o*PADs. In this approach, a fluidic architecture is patterned onto a single piece of paper, and then the paper is folded to produce the final device. This approach eliminates the need for photopatterning, cutting out individual layers of paper, aligning and taping them together, and filling the vias with cellulose powder. Keeping in mind that the main advantage of paper fluidic devices over those fabricated from plastic is their support of more complex fluidic functionality including both 2D and 3D topologies, manufacturing methods will have to be chosen carefully for compatibility with ultrahigh throughput to keep costs low enough to be competitive with present-day LFA technology.

In a previous paper focused on hollow-channel μPADs, we reported the first example of 3D wax patterning by integrating hemichannels into paper devices.[24] Recently, Li et al. used this approach to fabricate up to four independent layers in a 315 μm thick cellulose filter paper.[25] Here, we go further by providing a quantitative study and detailed physical description of wax impregnation into paper. The key point is that the initial amount of wax printed on the surface of the paper dictates its spreading characteristics. By carefully controlling both the amount of wax printed on the paper and the infusion of the wax into the paper, complex functional channel architectures are obtained in a single wax patterning step.

3D wax patterning retains the principal advantages of the wax patterning method (simplicity and speed) but offers additional design flexibility. Importantly, replacement of open channels with hemichannels in 3D *o*PADs reduces the number of layers required for a particular function by 50%. We also show that fully enclosed channels prevent liquid exchange between the interior and the exterior of the channel, thereby decreasing contamination risks and greatly reducing the rate of solvent evaporation, in addition to enabling lower limits of detection (through reduced loss of the analytical target) and improved separation performance (where relevant) due to reduced flow dispersion.

EXPERIMENTAL SECTION

Chemicals, Materials, and Equipment. Remazol brilliant blue R was purchased from Sigma-Aldrich (St. Louis, MO). Tris(1,10-phenanthroline) iron(II) sulfate (red dye) and tris(bipyridine)-ruthenium(III) chloride (orange dye) were purchased from Acros Organics (Morris Plains, NJ). 4′,6-Diamidino-2-phenylindole dihydrochloride (DAPI) was purchased from Life Technologies (Carlsbad, CA). Deionized water having a resistivity >18 MΩ·cm was used for all experiments (Milli-Q gradient system, Millipore, Bedford, MA). Devices were fabricated using either grade 1 (180 μm thick, 20 × 20 cm sheets) or 3MM (340 μm thick, 15 × 17.5 cm sheets) Whatman chromatography paper purchased from Fischer Scientific (Waltham, MA). A Xerox ColorQube 8570 printer was used for all wax printing.

Wax Transport Measurements. To measure the wax transport in the plane of the paper, a wax line (between 0.30 and 3.00 mm wide) was first printed on Whatman grade 1 chromatography paper. The paper was subsequently cut into 1 × 1 cm pieces so that a 1 cm long wax line spanned each piece. Next the paper pieces were heated on a hot plate (wax side up) set at 120 °C, and at specified time intervals individual pieces were removed, cooled, and imaged under a macroscope (Macroscope 25, 8 × 25, RF Inter-Science Co., Patchogue, NY). The width of the lines was then measured using a scale bar integrated into the macroscope.

The extent of wax movement perpendicular to the plane of Whatman 3MM chromatography paper was also measured. In this case, one side of the paper was entirely covered with wax, and then the paper was cut into 1 cm × 1 cm pieces. These pieces were heated on a hot plate (wax side up) at 120 °C for specified periods of time, and then they were removed one by one, cooled, and sectioned with a razor blade, taking care not to apply so much compression as to distort the wax imprint. The cross sections of the paper were examined using a microscope (Nikon AZ100).

Fabrication of Hemichannels. Hemichannels were fabricated in three steps. First, the wax patterns (see Figure S1a in the Supporting Information) were printed on the top and the bottom of Whatman grade 1 chromatography paper. To ensure proper alignment between the top and the bottom, the paper was fed into the printer manually. After the printing step, the paper was placed in an oven at 120 °C for

dx.doi.org/10.1021/la501212b | *Langmuir* 2014, 30, 7030−7036

45 s to melt the wax. The *o*PAD was then folded and pressed tightly between two transparent plastic holders using binder clips. Note that the wax floors of the hemichannels were fabricated using yellow wax, which provides contrast and hence simplifies alignment during folding.

Fabrication of Fully Enclosed Channels. The fully enclosed channels were printed on Whatman 3MM chromatography paper. The pattern printed on the top and bottom of the paper is shown in Figure S1b (Supporting Information). After the printing step, the paper was placed in an oven at 120 °C for 1 min to melt the wax and then cooled at 23 °C.

Water Transport Measurements. Water transport was measured in both open and fully enclosed channels. A 100.0 mm long × 5.0 mm wide open channel was fabricated using Whatman grade 1 chromatography paper. A fully enclosed channel of similar length and width was wax patterned on Whatman 3MM chromatography paper. Small openings (0.80 mm diameter) in the wax capping layer were spaced along the channel at 5.0 mm intervals to observe the progression of the solution inside the fully enclosed channel. The open and fully enclosed channels were dipped by one end into a solution containing a dark blue dye (1 mM Remazol Brilliant Blue R). The distance traveled by the dye along the channels was measured as a function of time. The experiments were carried out in a chamber set at 37 °C and 23% relative humidity.

RESULTS AND DISCUSSION

Transport of Wax. Scheme 1 shows the two steps involved in wax patterning. First, a wax pattern is printed on the paper substrate (Scheme 1, top row). Second, the wax is melted to initiate penetration into the paper substrate (Scheme 1, bottom row). The driving force that moves the molten wax through the paper is capillary action. The distance L wicked by a liquid in a porous medium during a time t is given by the following equation:[26]

$$L = S\sqrt{t} \tag{1}$$

where S is defined by eq 2.

$$S = \sqrt{\frac{\gamma d}{4\eta}} \tag{2}$$

Here, γ is the surface tension, d is the pore diameter, and η is the dynamic viscosity of the liquid. In the same manner as the diffusion coefficient characterizes the diffusion of a molecule in a given medium, the coefficient S characterizes the wicking of a liquid in a given porous medium.

In this study, the movement of the wax is divided into two spatial components: a lateral component, L_{xy}, corresponding to wicking in the paper plane (laterally), and a transverse component, L_z, corresponding to the wax wicking along a direction perpendicular to the paper plane. The lateral wicking leads to a broadening of the printed features as shown by the two micrographs in Figure 1. For a wax line, the extent of the broadening can be defined by eq 3.

$$L_{xy} = \frac{w_f - w_i}{2} \tag{3}$$

Here, w_i and w_f are the widths of the line before and after heating, respectively (see Figure 1). The measurement of L_{xy} is discussed in more detail in the Supporting Information (Figure S2).

The time dependence of lateral wax spreading as a function of w_i is shown in Figure 1. Here, the blue, red, and black points correspond to w_i = 3.00, 0.60, and 0.30 mm, respectively, and the gray points correspond to w_i = 0.30 mm printed at 50% grayscale. In all cases, two distinct time domains are observed. During the first 5−10 min, the wicking rate follows a square root dependence, as shown by the good agreement between the least-squares fit of a square root function (continuous blue line in Figure 1) and the first 10 min of experimental data (blue points in Figure 1). This observation is consistent with that predicted by eq 1 for capillary action and results in a value of S = 240 ± 60 μm·min$^{-1/2}$. Accordingly, this value of S can be used to predict and account for the broadening of a wax line during the initial design of μPADs.

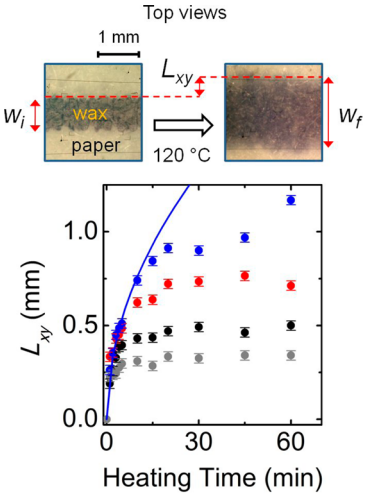

Figure 1. Micrographs showing the top views of a black wax line (w_i = 0.70 mm) before (left micrograph) and after (right micrograph) heating for 5.0 min at 120 °C. The plot shows how wax lines broaden in the plane of the paper (x, y) as a function of the heating time (T = 120 °C). The blue, red, and black data points correspond to wax lines with w_i = 3.00, 0.60, and 0.30 mm, respectively. The gray color corresponds to a 0.30 mm wide wax line printed at 50% grayscale. The values of L_{xy} are averaged over eight independently prepared devices. The error bars correspond to the uncertainty of the measurement (50 μm), which is greater than the standard deviations of the 8 measurements made for each point. The continuous blue line is a least-squares fit (R^2 = 0.965) of eq 1 (S = 240 ± 60 μm·min$^{-1/2}$) for the first 10 min of the experiment represented by the blue data points.

For heating times longer than t = 10 min, L_{xy} deviates significantly from the square root trend predicted by eq 1 and instead tends toward a limiting value, indicating that the wax line does not broaden at longer times. Figure 1 shows that smaller values of w_i give rise to smaller limiting values of L_{xy}. For example, a wax line that is initially 0.60 mm wide broadens to a maximum width of 0.75 mm, while a 0.30 mm wide wax line broadens to a maximum of 0.50 mm. Figure 1 also shows that a wax line printed at 50% grayscale broadens less than the same wax line printed at 100% grayscale (e.g., black data points). Micrographs of different percentage grayscale wax printing, prior to heating, are shown in Figure S3 (Supporting Information). These micrographs show that a lower grayscale leads to less wax printed atop the paper. We conclude, not surprisingly, that the presence of less wax leads to less wax broadening. This suggests that the plateaus in Figure 1, observed after ∼10 min of heating, arise from depletion of the wax initially printed on top of the paper.

An important consequence of the result shown in Figure 1 is that a judicious choice of the amount of wax printed can lead to new functionalities. For example, the two micrographs in Figure 2 show the transverse spreading of wax in Whatman 3MM chromatography paper. The first micrograph shows a very thin wax line (black) printed atop the paper (at the interface

dx.doi.org/10.1021/la501212b | *Langmuir* 2014, 30, 7030−7036

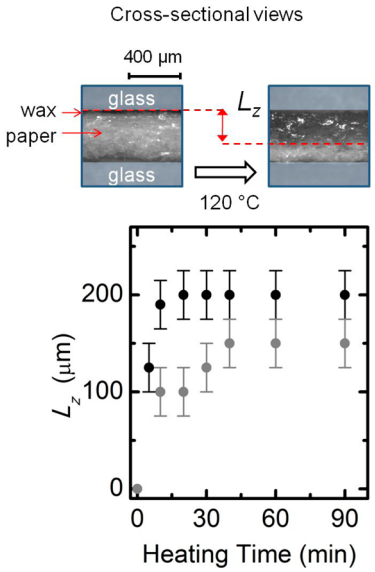

Figure 2. Micrographs showing a cross-sectional view of a 340 μm thick Whatman 3MM chromatography paper covered with black wax before (left micrograph) and after (right micrograph) heating for 15.0 min at 120 °C. The lower frame is a plot showing how the wax broadens perpendicular to the plane of the paper (L_z) as a function of the heating time (T = 120 °C). The black and gray data points correspond to paper initially fully (100% grayscale) and partially (50% grayscale) covered with wax, respectively. The values of L_z are averaged over eight independently prepared devices. The error bars correspond to the uncertainty in the measurement (50 μm), which is greater than the standard deviations of the 8 measurements made for each point.

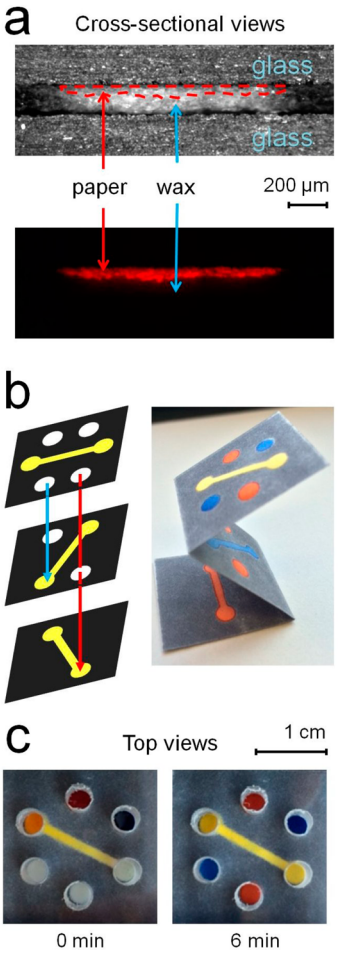

Figure 3. (a) Optical (top) and false color (bottom) fluorescence micrographs of the cross section of a hemichannel filled with a 1 mM DAPI dye solution. (b) Schematic illustration and photograph of a partially folded *o*PAD showing the relationship between the channels and vias. (c) Top view of a folded *o*PAD. At t = 0 min, the three top reservoirs were filled with orange, red, and blue dyes. The photograph on the right was taken 6.0 min after the reservoirs were filled.

between the upper glass piece and the top of the paper). The second micrograph shows that, after heating, the wax spreads only to a distance L_z, which is less than the 340 μm thickness of the paper. The plot in Figure 2 shows the relationship between L_z and heating time for paper initially covered with wax printed at 100% (black points) and 50% (gray points) grayscale. As already discussed for lateral wax spreading, transverse spreading is time dependent for t < ~10 min, but then reaches a constant value. This is because the initial amount of wax is insufficient to fill the full thickness of the paper. This result is consistent with previous findings that wax lines initially <0.30 mm thick do not form impermeable hydrophobic barriers throughout the thickness of 180 μm thick paper.[27] In the present case it is interesting to note that a decrease of the grayscale from 100% to 50% reduces the depth of wax penetration by ~25%. These relationships between the thickness and grayscale of wax lines is important, because it provides a simple way to control wax spreading and thus, as discussed next, makes it possible to create new types of functional channels in μPADs.

Hemichannels. The results shown in Figures 1 and 2 suggest the feasibility of fabricating structures of the sort shown in column b of Scheme 1, which we call hemichannels. This type of structure is fabricated by adjusting the amount of wax printed on the paper so that a hemicylinder of hydrophilic paper is surrounded by a wax barrier. Two cross-sectional views of a hemichannel are shown in Figure 3a. The top frame is an optical micrograph where the red dashed line indicates the position of the hemichannel. The wax walls to the left and right of the channel are black, indicating wax penetration through the thickness of the paper in these regions.

To enhance the contrast between the wax floor and the paper hemichannel, the latter was stained with a fluorescent dye (1 mM DAPI, bottom micrograph of Figure 3a). The dye only stains the unwaxed paper hemichannel, resulting in a brightly fluorescent section surrounded by black wax. Similar micrographs were used to measure the dimensions of the hemichannel. The results show that the dimensions of the hemichannel depend on the initial amount of printed wax, the heating time, and the temperature. For example, a 70 ± 10 μm tall hydrophilic channel sitting atop a 110 ± 10 μm thick wax floor is obtained (measured for three independently prepared hemichannels) using the following parameters: 60% yellow wax (see Table S1 in the Supporting Information), a heating time of 45 s, and a temperature of 120 °C.

The *o*PAD shown in Figure 3b was fabricated by wax patterning multiple hemichannels on a single sheet of paper and then folding it according to the origami method.[22] The photograph to the right of the scheme in Figure 3b shows an unfolded *o*PAD. The *o*PAD comprises three hemichannels, one on each of the three layers (shown in yellow in the scheme), and several vias (shown in white in the scheme). The thin blue

dx.doi.org/10.1021/la501212b | *Langmuir* 2014, 30, 7030−7036

and red lines in the scheme indicate the relationship of the vias after folding.

The photograph on the left side of Figure 3c is a top view of the folded *o*PAD immediately after introduction of orange, red, and blue dyes into three of the wells on the top layer of the device. The photograph on the right was taken 6 min later, and it shows that the dyes reach the opposite end of the respective channels without mixing. This result is important for two reasons. First, it demonstrates that liquid can flow via the hemichannel, and hence, these channels are functional. The second important result is that the dyes do not mix en route to the ends of the hemichannels. This means that the 110 μm thick wax floor of the hemichannels is impermeable to the aqueous dye solutions during filling. However, after ~15 min, small leaks are observed. This is typical of wax-printed features, and it sets an upper time limit for assays designed for wax-printed μPADs. It is reasonable to assume that this phenomenon depends upon and could be affected by both the choice of wax and the properties of the particular cellulosic paper chosen, in particular its surface energy.

Hemichannels provide some additional functionality compared to open channels. First, hemichannels reduce the number of layers required for fabrication of 3D μPADs. For example, Scheme 2a compares two 3D *o*PADs having identical functionalities. However, the one in the left column is fabricated using open channels, and the one on the right is composed of hemichannels. The open channels require an extra fully impermeable layer to prevent mixing of the solutions between adjacent layers. Because the required isolating layers are integrated into the hemichannels, the total number of paper layers required is reduced by a factor of 2.

We recently reported another useful application of hemichannels:[24,28] they were used as a component of a more complex structure called hollow channels. A three-dimensional perspective of a hollow channel is shown in Scheme 2b. In a single wax-patterning step, a paper device having both open channels (Scheme 1, column a) and hemichannels (Scheme 1, column b) is fabricated, and then the cellulose is removed from within the open channel to leave a hollow channel. After the device is folded into the desired configuration, the hemichannels cap the hollow channels and provide a hydrophilic surface along which an aqueous solution spontaneously wicks. The hemichannel function is very important for this application, because just a single hydrophilic wall in an otherwise hydrophobic channel is sufficient for capillary filling. In contrast, Whitesides and co-workers have shown that if all four walls of a hollow channel are hydrophobic, then high pressures are required to drive fluids.[29] For point-of-care applications, this is not a desirable situation.

Fully Enclosed Channels. A second example of the benefits of 3D wax patterning is provided by the type of fully enclosed channel represented in column c of Scheme 1. The fabrication of this device relies on two factors: the amount of wax printed and double-sided printing. As shown in Scheme 1, a fully enclosed channel is in essence a paper channel enclosed by four wax walls, the whole structure being contained within a single sheet of paper. Figure 4a shows a cross-sectional

Scheme 2. (a) Comparison of Open-Channel and Hemichannel Architectures and (b) Three-Dimensional Projection of a Closed Channel

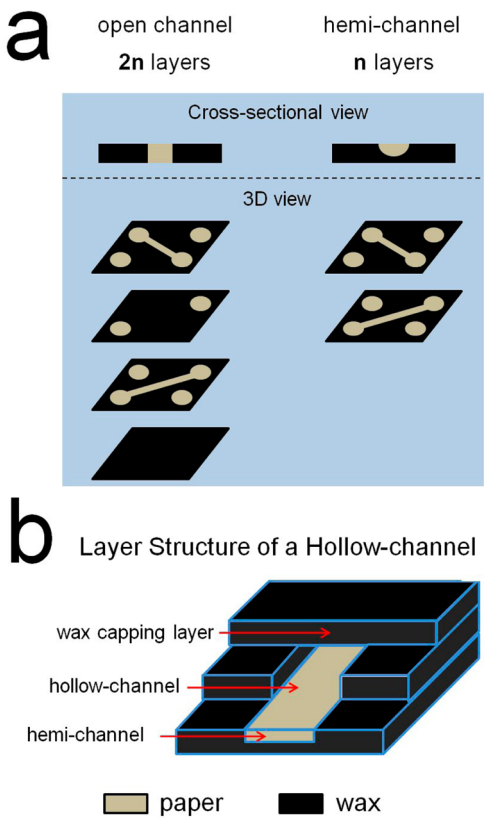

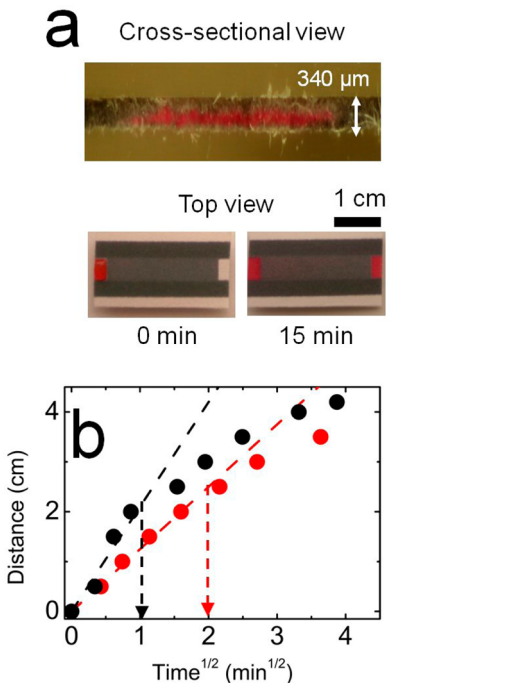

Figure 4. (a) Top micrograph: cross-sectional view of a fully enclosed channel filled with a red dye. Bottom photographs: top view of a fully enclosed channel. At t = 0 min, a red dye was introduced at the left end of the fully enclosed channel, and at t = 15 min the photograph on the right shows that the dye had flowed through the closed channel. (b) Distance traveled by water in a fully enclosed channel (red circles) and an open channel (black circles) as a function of $t^{-1/2}$. The experiment was carried out at 37 °C and at a relative humidity of 23%. The inlet of the channel was dipped into a reservoir of water to ensure a constant source of liquid.

dx.doi.org/10.1021/la501212b | *Langmuir* 2014, 30, 7030−7036

photograph of a fully enclosed channel fabricated in 340 μm thick Whatman 3MM chromatography paper. To increase the contrast with the black wax barriers, the enclosed paper channel is filled with a red dye. Under our experimental conditions, the open paper channel is 90 ± 10 μm tall, and two 140 ± 10 μm thick layers of wax enclose this unwaxed channel. The standard deviations in these measurements are derived from three independently prepared, fully enclosed channels (a representative micrograph used for these measurements is provided in Figure S4, Supporting Information). The uncertainty in the dimensions of the channels (~10%) arises from both the roughness of the paper matrix itself and the roughness of the cross-sectional cut required to measure the thickness.

To determine if liquid can wick through the paper channel, a red dye was introduced at the left end of the fully enclosed channel shown in Figure 4a (bottom left photograph). After 15 min another photograph was obtained (Figure 4a, bottom right photograph). The red coloration on the opposite end of the fully enclosed channel indicates that it is sufficiently hydrophilic to induce capillary flow. To test the impermeability of the capping wax layers, a strip of paper was pressed against a fully enclosed channel filled with a red dye for 30 min (Figure S5, Supporting Information). No red stain was observed on the paper strip, proving that the dye does not permeate the wax barrier.

The protection offered by the wax capping layers is important for several reasons. First, it prevents contamination of processes occurring in the channel. Second, it eliminates loss of low-concentration analytical target species that could worsen the limits of detection and analytical precision. Third, it reduces the rate of solvent evaporation. Figure 4b illustrates this point. It compares the distance wicked by an aqueous solution in a fully enclosed channel (red) and an open channel (black) as a function of the square root of time. The temperature (37 °C) and the relative humidity (23%) were carefully controlled to ensure reproducible results. The volume of liquid at the inlet of the channels was kept constant to ensure that the water supply does not limit the wicking rate. The dashed straight lines in Figure 4b are expected for capillary flow (eq 1). In the open channel, flow follows a $t^{1/2}$ dependence for ~1 min and then slows. In the fully enclosed channel, this $t^{1/2}$ dependence is followed for ~4 min. Similar experiments conducted at lower temperature (25 °C) and higher relative humidity (>90%) (Figure S6, Supporting Information) do not show deviation from the linear trend (on the same time scale) for either the open or fully enclosed channels. We conclude that the deviation from linearity in Figure 4b is due to evaporation of water as it makes its way down the channel. In other words, at the distal end of the open channel, the rate of evaporation exceeds the rate of replenishment from the reservoir after ~1 min. The effect is delayed by a factor of 4 in the fully enclosed channel. Hence, the capping wax layers slow evaporation but do not completely suppress it. Note that a similar observation has been reported by Schilling et al. for paper channels enclosed by laser-printer toner.[19]

SUMMARY AND CONCLUSIONS

Here we reported a simple method for fabricating 3D μPADs using wax printing, along with a fundamental understanding of the underlying enabling principles. Importantly, the method is based solely on the wicking properties of the wax and the chosen cellulosic paper and therefore does not require any reagents or fabrication steps beyond those required for normal 2D wax patterning. While preserving all the advantages of wax patterning (simplicity, rapidity, and low cost), this method enables fabrication of two new kinds of structures: hemichannels and fully enclosed channels. A particularly important property of the hemichannels is that they reduce, by 50%, the number of paper layers required to implement a given fluidic function, reducing the complexity of 3D μPADs. We also showed that fully enclosed channels resist water evaporation 4 times longer than open channels. In summary, control of wax processing simplifies device design without compromising function.

ASSOCIATED CONTENT

Supporting Information

Wax patterns used for the fabrication of the hemichannel-based *o*PAD and the fully enclosed channel, details on the measurement of L_{xy}, effect of the grayscale on the amount of printed wax, cross-sectional micrograph of a fully enclosed channel, permeability test for the fully enclosed channels, and water wicking rate under high humidity conditions. This material is available free of charge via the Internet at http://pubs.acs.org.

AUTHOR INFORMATION

Corresponding Author

*E-mail: crooks@cm.utexas.edu. Phone: 512-475-8674.

Notes

The authors declare no competing financial interest.

ACKNOWLEDGMENTS

We gratefully acknowledge sponsorship of this project by the Defense Advanced Research Projects Agency Diagnostics on Demand program (Contract HR0011-12-2-0003). We also thank the Robert A. Welch Foundation (Grant F-0032) for sustained research support.

REFERENCES

(1) Gubala, V.; Harris, L. F.; Ricco, A. J.; Tan, M. X.; Williams, D. E. Point of care diagnostics: status and Future. *Anal. Chem.* **2011**, *84*, 487−515.

(2) Parolo, C.; Merkoci, A. Paper-based nanobiosensors for diagnostics. *Chem. Soc. Rev.* **2013**, *42*, 450−457.

(3) Yetisen, A. K.; Akram, M. S.; Lowe, C. R. Paper-based microfluidic point-of-care diagnostic devices. *Lab Chip* **2013**, *13*, 2210−2251.

(4) Martinez, A. W.; Phillips, S. T.; Whitesides, G. M.; Carrilho, E. Diagnostics for the developing world: microfluidic paper-based analytical devices. *Anal. Chem.* **2010**, *82*, 3−10.

(5) Martinez, A. W.; Phillips, S. T.; Butte, M. J.; Whitesides, G. M. Patterned paper as a platform for inexpensive, low-volume, portable bioassays. *Angew. Chem., Int. Ed.* **2007**, *46*, 1318−1320.

(6) Cheng, C.-M.; Martinez, A. W.; Gong, J.; Mace, C. R.; Phillips, S. T.; Carrilho, E.; Mirica, K. A.; Whitesides, G. M. Paper-based ELISA. *Angew. Chem., Int. Ed.* **2010**, *49*, 4771−4774.

(7) Abe, K.; Suzuki, K.; Citterio, D. Inkjet-printed microfluidic multianalyte chemical sensing paper. *Anal. Chem.* **2008**, *80*, 6928.

(8) Li, X.; Tian, J.; Nguyen, T.; Shen, W. Paper-based microfluidic devices by plasma treatment. *Anal. Chem.* **2008**, *80*, 9131−9134.

(9) Fenton, E. M.; Mascarenas, M. R.; López, G. P.; Sibbett, S. S. Multiplex lateral-flow test strips fabricated by two-dimensional shaping. *ACS Appl. Mater. Interfaces* **2008**, *1*, 124−129.

(10) Lu, Y.; Shi, W.; Jiang, L.; Qin, J.; Lin, B. Rapid prototyping of paper-based microfluidics with wax for low-cost, portable bioassay. *Electrophoresis* **2009**, *30*, 1497−500.

(11) Mentele, M. M.; Cunningham, J.; Koehler, K.; Volckens, J.; Henry, C. S. Microfluidic paper-based analytical device for particulate metals. *Anal. Chem.* **2012**, *84*, 4474−4480.
(12) Ge, L.; Wang, S.; Song, X.; Ge, S.; Yu, J. 3D origami-based multifunction-integrated immunodevice: low-cost and multiplexed sandwich chemiluminescence immunoassay on microfluidic paper-based analytical device. *Lab Chip* **2012**, *12*, 3150−3158.
(13) Thom, N. K.; Yeung, K.; Pillion, M. B.; Phillips, S. T. "Fluidic batteries" as low-cost sources of power in paper-based microfluidic devices. *Lab Chip* **2012**, *12*, 1768−1770.
(14) Nie, Z.; Deiss, F.; Liu, X.; Akbulut, O.; Whitesides, G. M. Integration of paper-based microfluidic devices with commercial electrochemical readers. *Lab Chip* **2010**, *10*, 3163−9.
(15) Yan, J.; Ge, L.; Song, X.; Yan, M.; Ge, S.; Yu, J. Paper-based electrochemiluminescent 3D immunodevice for lab-on-paper, specific, and sensitive point-of-care testing. *Chem.—Eur. J.* **2012**, *18*, 4938−45.
(16) Wang, P.; Ge, L.; Yan, M.; Song, X.; Ge, S.; Yu, J. Paper-based three-dimensional electrochemical immunodevice based on multi-walled carbon nanotubes functionalized paper for sensitive point-of-care testing. *Biosens. Bioelectron.* **2012**, *32*, 238−243.
(17) Dungchai, W.; Chailapakul, O.; Henry, C. S. A low-cost, simple, and rapid fabrication method for paper-based microfluidics using wax screen-printing. *Analyst* **2011**, *136*, 77−82.
(18) Olkkonen, J.; Lehtinen, K.; Erho, T. Flexographically printed fluidic structures in paper. *Anal. Chem.* **2010**, *82*, 10246−50.
(19) Schilling, K. M.; Lepore, A. L.; Kurian, J. A.; Martinez, A. W. Fully enclosed microfluidic paper-based analytical devices. *Anal. Chem.* **2012**, *84*, 1579−1585.
(20) Maejima, K.; Tomikawa, S.; Suzuki, K.; Citterio, D. Inkjet printing: an integrated and green chemical approach to microfluidic paper-based analytical devices. *RSC Adv.* **2013**, *3*, 9258−9263.
(21) Martinez, A. W.; Phillips, S. T.; Whitesides, G. M. Three-dimensional microfluidic devices fabricated in layered paper and tape. *Proc. Natl. Acad. Sci. U.S.A.* **2008**, *105*, 19606−19611.
(22) Liu, H.; Crooks, R. M. Three-dimensional paper microfluidic devices assembled using the principles of origami. *J. Am. Chem. Soc.* **2011**, *133*, 17564−17566.
(23) Liu, H.; Xiang, Y.; Lu, Y.; Crooks, R. M. Aptamer-based origami paper analytical device for electrochemical detection of adenosine. *Angew. Chem., Int. Ed.* **2012**, *51*, 6925−8.
(24) Renault, C.; Li, X.; Fosdick, S. E.; Crooks, R. M. Hollow-channel paper analytical devices. *Anal. Chem.* **2013**, *85*, 7976−7979.
(25) Li, X.; Liu, X. Fabrication of three-dimensional microfluidic channels in a single layer of cellulose paper. *Microfluid. Nanofluid.* **2014**, *16*, 819−827.
(26) Washburn, E. W. The dynamics of capillary flow. *Phys. Rev.* **1921**, *17*, 273−283.
(27) Carrilho, E.; Martinez, A. W.; Whitesides, G. M. Understanding wax printing: a simple micropatterning process for paper-based microfluidics. *Anal. Chem.* **2009**, *81*, 7091−7095.
(28) Renault, C.; Anderson, M. J.; Crooks, R. M. Electrochemistry in hollow-channel paper analytical devices. *J. Am. Chem. Soc.* **2014**, *136*, 4616−4623.
(29) Glavan, A. C.; Martinez, R. V.; Maxwell, E. J.; Subramaniam, A. B.; Nunes, R. M. D.; Soh, S.; Whitesides, G. M. Rapid fabrication of pressure-driven open-channel microfluidic devices in omniphobic RF paper. *Lab Chip* **2013**, *13*, 2922−30.